Aero Maneuvering Dynamics and Control for Precision Landing on Titan[1],[2]

Marco B. Quadrelli, Aaron Schutte, Jasmine Rimani, Luca Ermolli
Jet Propulsion Laboratory, California Institute of Technology
4800 Oak Grove Dr., Pasadena, CA 91109
818-354-7548, marco.b.quadrelli@jpl.nasa.gov

Abstract— We have developed and tested several dynamic models of the parafoil system descending in Titan's atmosphere. These dynamic models include a progression from point mass models to rigid multibody models, including relative dynamics between canopy and payload. In these models, we have included wind models used for Titan simulation, and extrapolated wind gust models previously used for simulation in the Martian environment. We have also developed guidance and control techniques for autonomous parafoil turning in the adverse wind environment. Finally, and in order to improve the controller performance by reducing the uncertainty to environmental factors, we have also developed ways to estimate the Titan environmental parameters, i.e. the atmospheric density, and the wind magnitude, during the descent. A more complete and realistic simulation is being developed, which uses JPL's DSENDS Entry, Descent, and Landing Software framework.
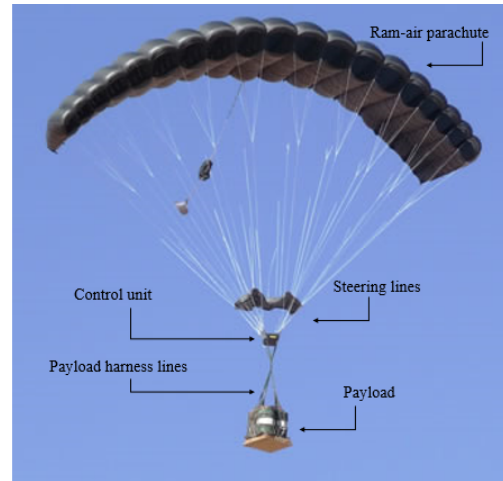
TABLE OF CONTENTS

Figure 1: Parafoil main components.
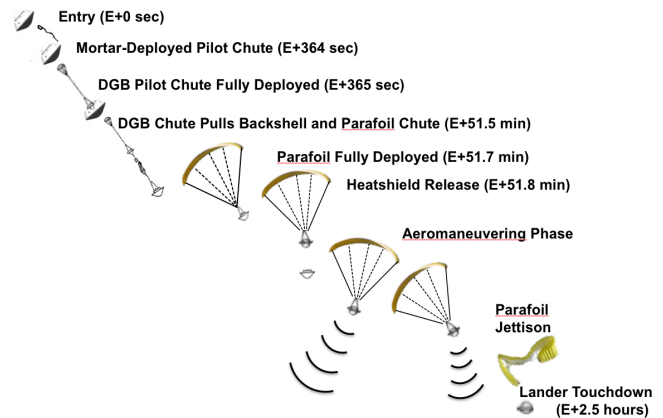

Figure 2. Notional Titan Lander Terminal Descent Trajectory.

1. INTRODUCTION

Saturn's moon Titan is likely the richest laboratory in the solar system for studying prebiotic chemistry, which makes studying its chemistry from the atmosphere to the surface one of the most important objectives in planetary science [1,2,4,5,6,7,8,9,10]. Studying Titan's organic chemistry requires landing to

sample and analyze fluids, dissolved species, and sediments from Titan's seas, lakes, tidal pools, or shorelines. Landing dispersions with existing technology are hundreds of kilometers wide, which precludes landing in any liquid body except the large seas at high northern latitudes. Low to medium cost missions require direct to Earth (DTE) communication; seasons on Titan now prevent such missions to northern seas for landings before the late 2030s. With these large landing dispersions, access to shorelines or other smaller features on Titan, which may present liquid-solid interfaces or more dynamic environments conducive to more chemical evolution, is only conceivable by relying on wind drift after landing on large seas. Therefore, there is a critical need for more precise landing capability to explore the unique potential for prebiotic chemistry on Titan's surface.

The focus of our work is on technology development to substantially reduce Titan lander delivery error. By far the greatest contribution to this error in past Titan mission designs has been long parachute descent phases (~ 2.5 hours) from high altitudes (~ 150 km) in high winds with large wind uncertainties; therefore, addressing error during parachute descent is the key to enabling precision landing. Lowest delivery error would be achieved with a multi-stage parachute system, with an unguided drogue parachute that descends rapidly through altitudes with high winds, followed by a guided parafoil (Figure 1) with a high glide ratio that flies out position error at lower altitudes. Parafoil deployment at altitudes up to 40 km, where proven descent camera technology could see the surface to enable position estimation, could reduce delivery error by 100 km or more. A notional terminal descent trajectory is shown in Figure 2. The main risk areas in this concept are uncertainty in the precision of descent navigation and in parafoil guidance and control (G&C) performance. The only possible source of adequate position knowledge is onboard terrain-relative navigation (TRN), using a camera to recognize and track features of Titan's surface during descent. TRN for precision landing on Mars is now at TRL 6 and is expected to be at TRL 9 by 2020 as part of the 2020 Mars rover mission. Leveraging that development has potential to make TRN available for Titan at relatively low cost in a relatively short timeframe; however, factors unique to Titan require changes to the design of the TRN system. Parafoil aerodynamic performance has not been characterized yet for the dense Titan atmosphere and parafoil G&C algorithms must be adapted to unique characteristics of Titan missions. As part of this effort, and leveraging past work [1,2,3,4,5,6,7,8,9,10,11,12,13,14], we have been developing a simulation of end-to-end EDL performance and using the simulation to estimate and optimize expected landing dispersion, with the goal of showing feasibility of reducing delivery error by at least 100 km compared to Huygens-like descent. Success in that endeavor would enable using this capability for Titan missions as early as launch opportunities in the late 2020s. To achieve Titan precision landing in this timeframe requires starting this technology development now.

3. TITAN'S ENVIRONMENT

Titan's low gravity (1/7th of Earth's) and dense, tall atmosphere (4 times denser than Earth's at the surface and 5 times Earth's scale height) has led to EDL architectures with steep entry (e.g. -65°) lasting a few minutes, followed by long parachute descent (~2.5 hours) from high altitude (~150 km) [1,2]. The Huygens probe experienced high winds at high altitude, which caused it to drift about 160 km east after parachute deployment [4]. Global circulation models predict much larger zonal (east-west) than meridional (north-south) winds, except near the poles, that vary substantially with latitude and season [17]. Thus, 99% confidence landing ellipses are typically very eccentric, with east-west oriented major axes roughly 200 to 500 km long, but only 50 to 100 km wide [2,11]. Achieving our objectives would enable flying to the center of a 200 km ellipse; it would also enable flying the full width of the narrow axis of all previous ellipses, which could enable landing near linear features paralleling the long axis of the ellipse, like shorelines. "Lorenz et al" formulate an exponential wind model in [17] that can describe the atmosphere of the poles in late summer. The climate can change abruptly with latitude and season: this model could degrade in validity at different seasons or latitudes. However, we will use this wind formulation in all the simulations reported in this paper as a reference wind disturbance model to develop and test our models. The wind is divided by zonal wind and meridian wind: the first is a high intensity wind that can heavily affect the trajectory, the latter is a disturbance wind around 1-2 m/s. The zonal wind model (west-east direction) is realized for a latitude of 80° with the following model, where W_{300} : speed of wind at 300 km, z_0: reference altitude, z: altitude at which we are evaluating the wind, and L: length scale:

$$W = \frac{W_{300}}{1 + e^{\frac{z_0 - z}{L}}} \quad m/s$$

(1)

From [17] we can derive the wind environment as well as density and gravity from the surface up to 170 km. The density and gravity of Lorenz is derived from [16], usually referred as the "Yelle model", as:

$$\rho = 5.43 * e^{\frac{-0.512*h}{1000}} \quad kg/m^3$$

(2)

3. CHALLENGES OF USING A PARAFOIL SYSTEM

There are several types of steerable parachutes with a wide range of glide ratios and steerability [14]. Ram-air parafoils are the most attractive type for this application, due to their high glide ratios, compact storability, high level of maturity, and the extensive experience in NASA and industry in their use in autonomous, precision delivery applications. Parafoils have a ram-air inflated, double membrane airfoil cross-section (Figure 3) and are equipped for steering by means of wing tip or trailing edge lines. Pulling the lines creates either aileron or spoiler effects, or wing-tip angle of attack changes. Terrestrial landing sites are usually point targets on solid ground. Wind velocity can be high, with large uncertainty in direction and magnitude. G&C algorithms seek to minimize the "miss distance" between the target point and the actual landing site. These algorithms typically have four stages: 1) turn to the target, 2) fly toward the target, 3) if necessary, conduct loitering maneuvers ("energy management") to avoid overshooting the target, and 4) perform a terminal guidance maneuver to manage touchdown velocity, which may involve turning into the wind and flaring the parafoil to reduce velocity just before touchdown [14,27,28,29]. With GPS and an IMU for navigation and with good wind knowledge, miss distances of < 100 m are achievable. Real-time onboard wind estimation has been studied to reduce error due to wind uncertainty [22, 23, 24].
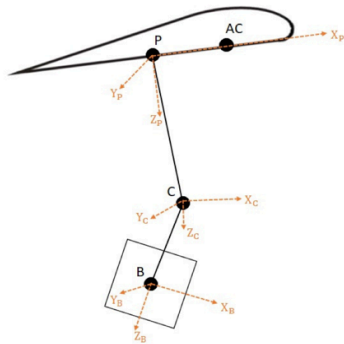

Figure 3. One of the vehicle models considered in our study.

Constructing parafoil canopies, suspension and control lines, and actuators suitable for the Titan environment is well understood engineering, with some heritage from the Huygens probe. Achieving successful deployment and inflation of parafoils on Titan is not expected to be a major challenge, because it will occur in Mach number and dynamic pressure regimes similar to applications on Earth. These issues are not addressed in our proposed work. The unique challenges of using a parafoil to land on Titan are as follows:

- The different gravity and atmospheric density cause different parafoil aerodynamic performance, which has never been modeled.

- Initial drogue deployment must occur around 140 km AGL, and high winds at high altitudes cause very large dispersion during long parachute descents. We use an unguided drogue to descend quickly to a region of lower wind, then deploying a parafoil to obtain control authority. Optimal descent rates and deployment altitudes for the drogue and parafoil to minimize dispersion are unknown and depend on wind profiles and touchdown velocity constraints.

- Winds are highly variable; however, winds are predominantly zonal, the variability is largely in the zonal direction, and the wind velocity profile below about 50 km AGL has a well-defined shape [17]. This simplifies the design of algorithms for guidance and onboard wind estimation.

- Landing in lakes or seas and preventing the parafoil from falling on the lander (entrapment) places unique requirements on the design of terminal descent. This requires the guidance algorithm to maintain view of land for much of the descent to enable TRN, choose when to turn over the liquid body, and choose whether or not to follow the shoreline. Since winds below 5 km are on the order of 1 m/s, the terminal guidance stage may not need to turn into the wind; however, the high glide ratio may require a different approach to reduce horizontal velocity for splashdown.

- Camera-based navigation requires a stable imaging platform [15]. Based on the Huygens probe experience and previous studies of parachute dynamics [3,6,7,11], we do not expect this to be a problem.

$AR = 2.5$	Aspect Ratio
$b = \sqrt{S * AR}$	Parafoil Wingspan
$c = \sqrt{S/AR}$	Parafoil Chord
$h = 0.14 * c$	Parafoil height
$R/b = 0.6 \div 0.8$	Line-length-to-span ratio
$\epsilon = b/2/R$	Anhedral angle

Table 1. Parafoil preliminary design parameters.

4. APPARENT MASSES

The parafoil model includes the dynamics of the canopy (assumed already inflated), and the suspended payload (see Figure 3). Table 1 summarizes the basic parafoil geometric parameters. When a body is moving in a fluid, it sets the fluid into motion. Thus, the motion generates a pressure field around the body that we call apparent mass pressure. For every moving body in fluid, we can define a mass ratio between the mass of the system and the air mass shifted by the vehicle. For an airplane, the apparent mass is negligible, for a parafoil, the apparent mass heavily characterizes the dynamics of the ram-air. The dynamic model also includes the apparent mass effects, which are modeled as added mass and inertia tensors. Figure 4 and Figure 5 show a geometric representation of the apparent masses and inertias for an inflated canopy [19]. To evaluate the entity of the apparent mass, we usually use a formulation similar to the one in equation (3).

$$M_r = \frac{m}{\rho * S^{\frac{2}{3}}}$$

(3)

The ratio is usually in the order of 0.8 on Earth environment and around 7 for a parafoil flying in Titan atmosphere. If the parafoil is thought as inflated, the apparent mass tensor M_f and the apparent inertia tensor I_f are defined as [7]:

$$M_f = \begin{bmatrix} A & 0 & 0 \\ 0 & B & 0 \\ 0 & 0 & C \end{bmatrix}$$

$$I_f = \begin{bmatrix} I_a & 0 & 0 \\ 0 & I_b & 0 \\ 0 & 0 & I_c \end{bmatrix}$$

(4)

where:

$$A = 0.666 * \rho * \left(1 + \frac{8}{3} * a^{*2}\right) * t^2 * b$$

$$B = 0.267 * \rho * \left(1 + 2 * \frac{a^{*2}}{t^{*2}} * AR * (1 - t^{*2})\right) * t^2 * c$$

$$C = 0.785 * \rho * \sqrt{1 + 2 * a^{*2} * (1 - t^{*2})} * \frac{AR}{1 + AR} * c^2 * b$$

$$I_a = 0.055 * \rho * \frac{AR}{1 + AR} * c^2 * b^3$$

$$I_b = 0.0308 * \rho * \frac{AR}{1 + AR} * [1 + \frac{\pi}{6} * (1 + AR) * AR * a^{*2} * t^{*2}] * c^4 * b$$

$$I_c = 0.0555 * \rho * (1 + 8 * a^{*2}) * t^2 * b^3$$

$$AR = \frac{b}{c} \quad t^* = \frac{t}{c} \quad a^* = \frac{a}{b}$$

(5)

where b,c,t and a are respectively the parafoil wingspan, the parafoil chord, the parafoil thickness and the parafoil height.
Figure 6 shows a plot of the apparent masses during as a function of altitude on Titan for a small parafoil.
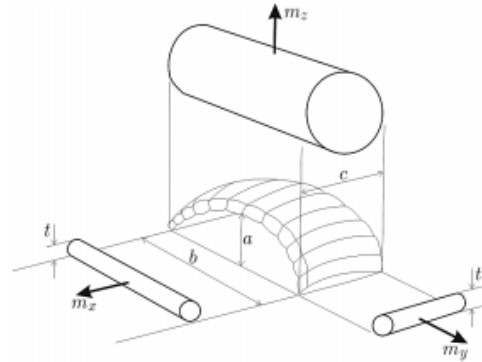

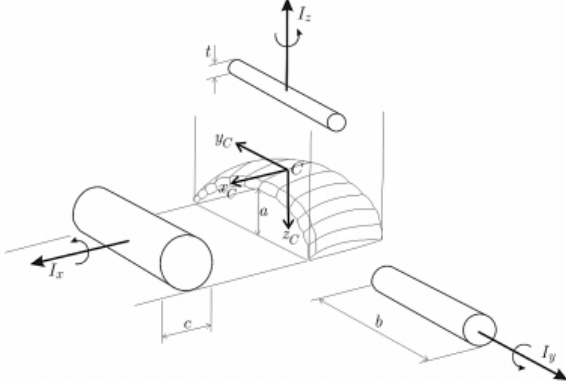Figure 4. Apparent masses representation for an inflated canopy [19].

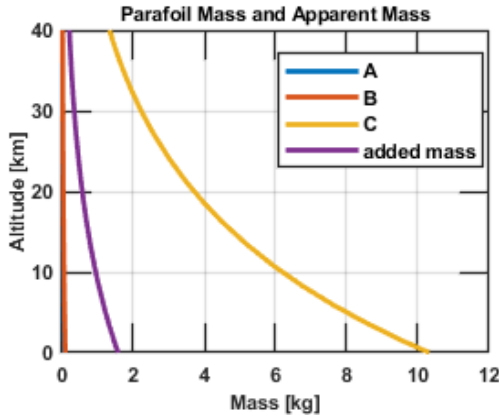Figure 5. Apparent inertias representation for an inflated canopy [19].

Figure 6: Apparent masses entity during Titan descent for a small parafoil.

5. AERODYNAMIC COEFFICIENTS

To find the aerodynamics of the parafoil in the Titan environment, it is advisable to compute the required database from a CFD (computational Fluid Dynamics) analysis [14]. However, in this preliminary phase of the project, we should find an easier and more straightforward way to obtain the aerodynamic coefficients. We can compute the coefficients in an Earth environment and then scale them for Titan's atmosphere. From [20,25,26] we can derive the values of force coefficients of the parafoil from the lifting line theory: unfortunately, that method overestimated the lift and underestimated the drag (the estimation is based only on the wing profile). The mathematical expressions from [14,18,21,22] become very useful if we aim to estimate the control derivatives for the ram-air $\{C_{L_{ds}}, C_{D_{ds}}, C_{m_{ds}}, C_{n_{da}}, C_{l_{da}}\}$. To estimate the aerodynamic coefficients of a certain wing-shape we can use a panel method: we will obtain a consistent set dependent on the angle of attack and on the airspeed. The tool "Tornado" [20] enables to analyze different

wings with different profiles: for the parafoil an usual profile is the CLARK-Y. However, the drag data obtained from the method must be uploaded with some value typical of the parafoil system. The parafoil profile is cut to form an inlet that permits to inflate the canopy: inside the ram-air is trapped an air mass called added mass. The associated drag is called inlet drag. Table 2 shows the additional drag contributions for the parafoil aerodynamics. Table 3 summarizes the aerodynamic coefficients used in the simulations [25,26]. Table 4 shows the parafoil and payload dimensions used in the simulations. The aerodynamic coefficients used in flight mechanics can be mathematically expressed as:

$$C_D = C_{D0} + C_{D\alpha^2}\alpha^2 + C_{D\delta_s}\delta_s$$
$$C_Y = C_{Y\beta}\beta$$
$$C_L = C_{L0} + C_{L\alpha}\alpha + C_{L\delta_s}\delta_s$$
$$C_X = \frac{(-C_D u_p + C_L w_p)}{V_P}$$
$$C_Z = \frac{-C_D w_p - C_L u_P}{V_P}$$
$$C_l = C_{l\beta}\beta + \frac{b}{2V_P}C_{lp}p_P + \frac{b}{2V_P}C_{lr}r_P + C_{l\delta_a}\delta_a$$
$$C_m = C_{m0} + C_{m\alpha}\alpha + \frac{c}{2V_P}C_{mq}q_P$$
$$C_n = C_{n\beta}\beta + \frac{b}{2V_P}C_{np}p_P + \frac{b}{2V_P}C_{nr}r_P + C_{n\delta_a}\delta_a$$
$$\boldsymbol{F_{a_B}} = \frac{1}{2}\rho V_B S_B C_{D_B}\begin{bmatrix} u_B \\ v_B \\ w_B \end{bmatrix}$$
$$\boldsymbol{M_{a_P}} = \frac{1}{2}\rho V_P^2 S \begin{bmatrix} bC_l \\ cC_m + x_{pa}C_z \\ bC_n \end{bmatrix}$$
$$\boldsymbol{F_{a_P}} = \frac{1}{2}\rho V_P^2 S \begin{bmatrix} C_X \\ C_Y \\ C_Z \end{bmatrix}$$

(6)

$C_{D_{inlet}} = 0.5 * h/c$	Inlet drag (c=profile chord, h=inlet height)
$C_{D_{lines}} = 0.019$	Drag relative to the rise lines for a small parafoil.
$C_{D_{roughness}} = 0.004$	Drag relative to the parafoil surface roughness

Table 2. Additional drag contributions for the parafoil aerodynamics.

$C_{D0} = 0.25$	$C_{D\alpha} = 0.12$	$C_{D_{\delta_s}} = 0.1$	
$C_{Y\beta} = -0.23$			
$C_{L0} = 0.091$	$C_{L\alpha} = 0.90$	$C_{L_{\delta_s}} = 0.15$	
$C_{m0} = 0.35$	$C_{m\alpha} = -0.72$	$C_{mq} = -1.49$	
$C_{l\beta} = -0.036$	$C_{lp} = -0.84$	$C_{lr} = -0.082$	$C_{l\delta_a} = -0.0035$
$C_{n\beta} = -0.0015$	$C_{np} = -0.082$	$C_{nr} = -0.27$	$C_{n\delta_a} = 0.0115$
$C_{D_{payload}} = 0.4$			

Table 3. Aerodynamic coefficients used in the simulations [25,26].

6. SYSTEM EQUATIONS OF MOTION

The six-degrees of freedom model is usually used to develop and test Guidance, Navigation and Control algorithms: the parafoil-payload system is a rigid 3D body with linear velocities, attitude and angular rates resulting from the motion of the two main components. Several models have been developed in literature [21,22,23,24,27,28]. In our case this approximation of the true dynamics can be useful to study the system characteristics with few inputs on the parafoil size, shape and dimension.

$b = 3.07\ m$	Parafoil wingspan
$c = 1.02\ m$	Parafoil aerodynamic chord
$t = 0.075$	Parafoil thickness
$a = 0.164\ m$	Parafoil height
$R = 1.84\ m$	Parafoil line length (from parafoil to confluence point)
$\mu = -12\ deg$	Rigging angle
$\epsilon = 47.74\ deg$	Anhedral angle
$l_{ha} = 1\ m$	Harness length
$m_p = 1.4\ m$	Parafoil mass
$\sigma = 0.45$	Sigma aerial density
$\delta_{max} = 0.16\ m$	Maximum trailing edge deflection
$z_s = 0.5\ m$	Payload height
$x_s = 0.5\ m$	Payload length
$y_s = 0.5\ m$	Payload width
$m_s = 200\ kg$	Payload mass

Table 4. Parafoil and payload dimensions used in simulations.

For the six degrees of freedom system, the equations of motion are:

$$\begin{bmatrix} (m+m_e)*I_{3x3} + M_f' & -M_f'*S(r_{BM}) \\ S(r_{BM})*M_f' & I + I_f' - S(r_{BM})*M_f'*S(r_{BM}) \end{bmatrix} * \begin{bmatrix} \dot{u} \\ \dot{v} \\ \dot{w} \\ \dot{p} \\ \dot{q} \\ \dot{r} \end{bmatrix} = \begin{bmatrix} F \\ M \end{bmatrix}$$

$$F = F_a^p + F_a^s + F_g + F_b^p - (m+m_e)*S(\omega)*\begin{bmatrix} u \\ v \\ w \end{bmatrix} - S(\omega)*M_f'$$
$$*\left(\begin{bmatrix} u \\ v \\ w \end{bmatrix} - S(r_{BM})*\begin{bmatrix} p \\ q \\ r \end{bmatrix}\right) + S(\omega)*M_f'*R_{bn}*W$$

$$M = M_a + M_b^p + S(r_{BM})*F_a^p + S(r_{BS})*F_a^s -$$
$$S(\omega)*I*\begin{bmatrix} p \\ q \\ r \end{bmatrix} - S(\omega)*I_f'*\begin{bmatrix} p \\ q \\ r \end{bmatrix} - S(r_{BM})*S(\omega)*M_f'$$
$$*\left(\begin{bmatrix} u \\ v \\ w \end{bmatrix} - S(r_{BM})*\begin{bmatrix} p \\ q \\ r \end{bmatrix} - R_{bn}*W\right)$$

$$\begin{bmatrix} \dot{\phi} \\ \dot{\theta} \\ \dot{\psi} \end{bmatrix} = \begin{bmatrix} 1 & \sin(\phi)*\dfrac{\sin(\theta)}{\cos(\theta)} & \cos(\phi)*\dfrac{\sin(\theta)}{\cos(\theta)} \\ 0 & \cos(\phi) & -\sin(\phi) \\ 0 & \sin(\phi)*\dfrac{1}{\cos(\theta)} & \cos(\phi)*\dfrac{1}{\cos(\theta)} \end{bmatrix} * \begin{bmatrix} p \\ q \\ r \end{bmatrix}$$

$$\begin{bmatrix} \dot{x} \\ \dot{y} \\ \dot{z} \end{bmatrix} = R'_{bn} * \begin{bmatrix} u \\ v \\ w \end{bmatrix}$$

(7)

where: "m" is the overall system mass; "m_e" is the added mass: the mass trapped inside the inflated parafoil. There are different expressions to evaluate it and they heavily depend on the parafoil shape. In our model, the added mass, is defined as in [9] using the profile area "$0.09 * c^2$ "."M_f'" is the parafoil apparent mass tensor rotated by the rigging angle; "I_f'" is the parafoil apparent inertia tensor rotated by the rigging angle; "W" is the wind vector expressed in NED (North-East-Down) frame; "$S(r_{BM})$" is the skew-symmetric matrix that replace the vector product $r_{BM} \times$. r_{BM} is the vector that points from the origin of the body reference frame to the apparent mass center of gravity of the parafoil.;"$S(r_{BS})$" is the skew-symmetric matrix that replace the vector product $r_{BS} \times$. r_{BS} is the vector that points from the origin of the body reference frame to the payload mass center; "F_a^p" is the parafoil aerodynamic force vector; "M_a^p" is the parafoil aerodynamic moment vector; "F_a^s" is the payload aerodynamic force vector; F_g" is the system weight force; "F_b^p" is the buoyancy force, upward force given by the parafoil added mass. It is small, but it can contribute to the overall balance of moments due to the large distance between the canopy mass center and the overall body center of gravity. More details on the model derivation can be found in [25,26].

7. SYSTEM STABILITY

A parafoil plus payload system is an inherently stable system, both longitudinal and latero-directional modes are stable, with a negative real part of the state matrix eigenvalues [14]. Usually they do not need any stability augmentation system, their dynamics is slow and winds disturbance is kept in account during the motion planning. This is shown in Table 5 and Figures 7a and 7b. Figures 7a and 7b show the longitudinal root locus of a parafoil and payload system. Table 5 shows the eigenvalues of typical modes of parafoil and payload system

Motion Mode	Eigenvalues	Period T [s]	Damping Ratio ξ
Short Period	-2.61±4.7i	1.3	0.49
Phugoid	-0.0855±0.004i	11	~1
Dutch Roll	-0.0715±0.145i	14	0.44
Roll Subsidence	-4.7	0.3	-
Spiral Mode	-3.8	0.2	-

Table 5. Eigenvalues of typical modes of parafoil and payload system
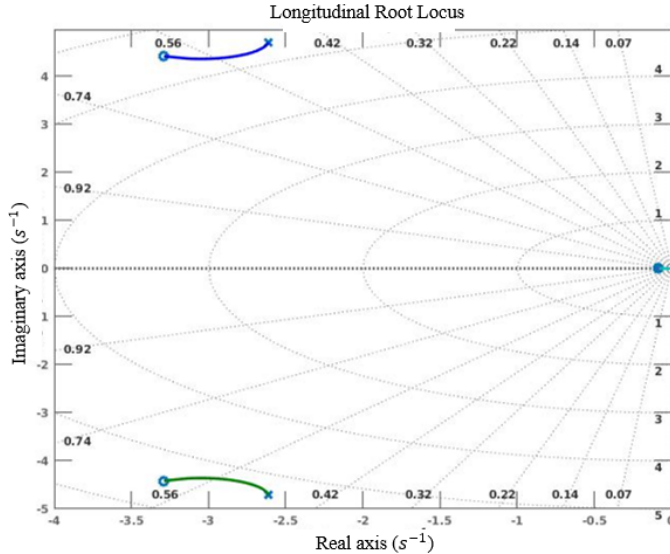

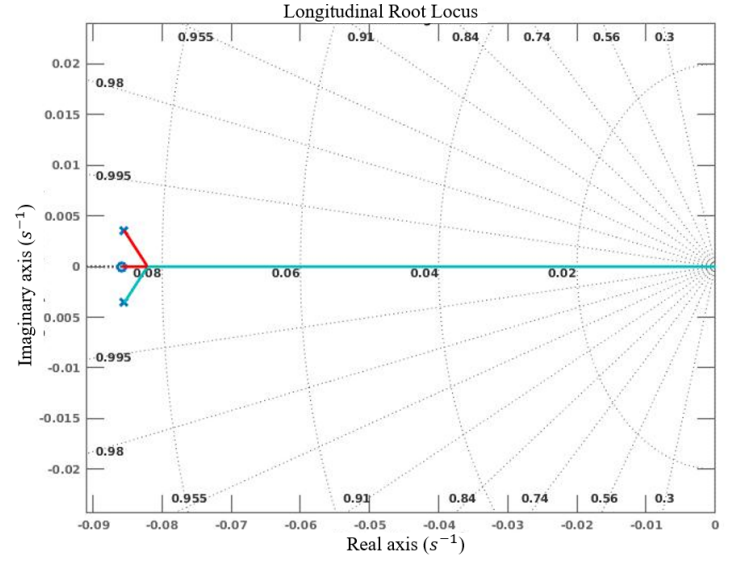Figure 7a. Longitudinal root locus of parafoil and payload system.

Figure 7b. Longitudinal root locus of parafoil and payload system, phugoid mode detail.

8. APPROACH FOR AUTONOMOUS DESCENT

Other authors have worked on autonomous parafoil descent [21,22,23,24,27,28,29]. Titan's distance of 10 AU from the sun and its strong atmospheric scattering and absorption imply low light levels near the surface and inability to obtain sharp images from high altitudes. The Huygens probe included a descent camera with a CCD imager using a spectral band of 660-1000 nm (Descent Imager/Spectral Radiometer, or DISR) [7], which saw the surface clearly below about 40 km AGL; attitude wobble of the probe was low enough to allow blur-free images with exposure times of ~7 to 40 milliseconds with f/2.5 optics [7,8,9,15]. Studies of parachute dynamics for the Huygens probe [2] and other missions [11,12,13] also imply that acceptable descent image quality is possible on Titan with practical exposure times for unguided parachutes, though this needs to be confirmed for guided parafoils.
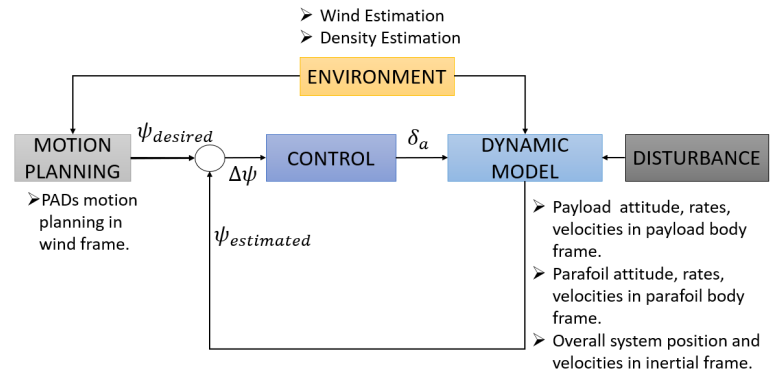

Figure 8. GN&C block diagram.

To see the surface clearly from above 40 km may require a camera operating at longer wavelengths, which appears to be unnecessary. Terrain Relative Navigation (TRN) provides position knowledge for parafoil guidance by matching descent images to map images obtained by prior missions. Good attitude, azimuth, and altitude knowledge is valuable to constrain initial image matching; once this is accomplished, ongoing image matching during descent is adequately constrained by previous state estimates and enables updating estimates of all elements of the navigation state vector. An Inertial Measurement Unit (IMU) is used to provide attitude and azimuth knowledge. The IMU used during EDL in the MSL mission [11] gives a lower bound on IMU error for performance modeling here; we assess sensitivity to IMU quality by varying this model. The Huygens probe had a radar altimeter designed to operate from 60 km to 150 m AGL with an error of 2.4%, though in-flight operation it detected the surface beginning at 45 km [1,2]; this provides a suitable initial altimetry performance model here. A block diagram of the GN&C (Guidance, Navigation, and Control) functions is shown in Figure 8.

9. WIND AND DENSITY ESTIMATORS

In these models, we have included wind models used for Titan simulation, and extrapolated wind gust models previously used for simulation in the Martian environment [12,13]. Part of this research was to develop models for a high precision delivery system on Titan environment, the other part is focused on how to use those models in a possible flight scenario in which Titan winds will make the parafoil drift away from target and some maneuvering will be required to land on spot. In this section a guidance navigation and control system will be analyzed for prove the capability of the models in plausible operational conditions and to lay the foundation of this kind on analysis. In PAD (Parafoil Autonomous Descent) GN&C [14], some important assumptions are made to simplify the equation and the approach of the trajectory definition: a) The sideslip angle β is small so that we can confound heading angle and yaw angle $\chi_{wind\,ref\,frame} \cong \psi_{NED}$; b) The wind is usually considered consistent only along the x-axis; c) The PADs should land against the wind (downwind). This will prevent payload roll-over, will decrease the landing speed and will permit a flare maneuver. The environmental conditions should affect the planned trajectory and the parafoil performance during descent. The true guidance system should re-plane the trajectory every interval of time to consider the strong wing uncertainties during descent. During

flight the wind can be estimated from the airspeed lecture of the Pitot as $\boldsymbol{W} = \boldsymbol{V_{NED}} - \boldsymbol{V_{airspeed}}$, and the IMU (Inertial Measurement Unit) will give the system linear velocities as output. These readings are affected by a noisy environments and errors: the values must be filtered to find a reliable quantity to use to plane the needed corrective maneuver, as follows:

$$\dot{x}_m = \dot{x}_{dynamic\,model} + \sigma_{\dot{x}} * p_{\dot{x}}$$
$$\dot{y}_m = \dot{y}_{dynamic\,model} + \sigma_{\dot{y}} * p_{\dot{y}}$$
$$\dot{z}_m = \dot{z}_{dynamic\,model} + \sigma_{\dot{z}} * p_{\dot{z}}$$
$$V_{am} = V_{airspeed} + \sigma_{airspeed} * p_{aispeed}$$
$$\gamma_{am} = \gamma_a + \sigma_{flightpath} * p_{flightpath}$$
$$\chi_{am} = \chi_a + \sigma_{heading} * p_{heading}$$

$$(8)$$

The $\{p_{\dot{x}}, p_{\dot{y}}, p_{\dot{z}}, p_{aispeed}, p_{flightpath}, p_{heading}\}$ are random numbers normally distributed. We used this expedient to simulate noisy wind measurements:

$$w_{x_m} = \dot{x}_m - V_{am} * \cos(\chi_{am}) * \cos(\gamma_{am})$$
$$w_{ym} = \dot{y}_m - V_{am} * \sin(\chi_{am}) * \cos(\gamma_{am})$$
$$w_{z_m} = \dot{z}_m - V_{am} * \sin(\gamma_{am})$$

$$(9)$$

To filter the wind evaluations, we can use a "recursive mean value estimation", a filter (e.g. Nonlinear Estimation Filter) or a predictive method that propagate the wind profile up to ground level (but it can be quite expensive in terms of computational power) [14]. We chose to use the "recursive mean value estimation" because it leads to simple formulation, and reliable results and works throughout all the GNC simulation (see Table 6).

0.1 s	Wind sampling step
0.002%	Mean error along the trajectory between exponential wind profile and estimated wind profile (derived from [5])
20%	Max error along all the trajectory between exponential wind profile and estimated wind profile.

Table 6. Recursive mean values wind estimation main prospects.

In literature there are some example of a standard "recursive mean value estimation" method for

autonomous parafoils in Earth environment. The classic formulas are reported in [14].

$$\bar{w}_{x_{k+1}} = (k * \bar{w}_{x_k} + w_x)/(k+1)$$
$$\bar{w}_{y_{k+1}} = (k * \bar{w}_{y_k} + w_y)/(k+1)$$

$$(10)$$

The expression (10) is useful if the wind environment doesn't change abruptly during the simulated scenario: in our case the longitudinal wind changes in its intensity during the descent from 40 km. An update formulation that considers only the previous 100 steps to evaluate the mean wind and detach errors from propagating. The algorithm for the wind estimator is as follows:

If $i \leq k_1$
$$\bar{w}_{x_{k+1}} = (k * mean(\bar{w}_{x_k}) + w_x)/(k+1)$$
$$\bar{w}_{y_{k+1}} = (k * mean(\bar{w}_{y_k}) + w_y)/(k+1)$$
If $i > k_1$
$$\bar{w}_{x_{k+1}} = (k * mean(\bar{w}_{x_k}(i - k_1:i)) + w_x)/(k+1)$$
$$\bar{w}_{y_{k+1}} = (k * mean(\bar{w}_{y_k}(i - k_1:i)) + w_y)/(k+1)$$

$$(11)$$

Figures 9 and 10 respectively show the zonal and meridian wind estimates during the descent, comparing the wind measured by the on-board instruments, the wind from Huygens, and the estimated wind components.
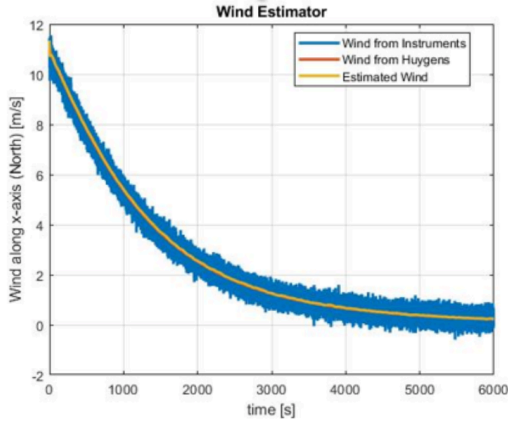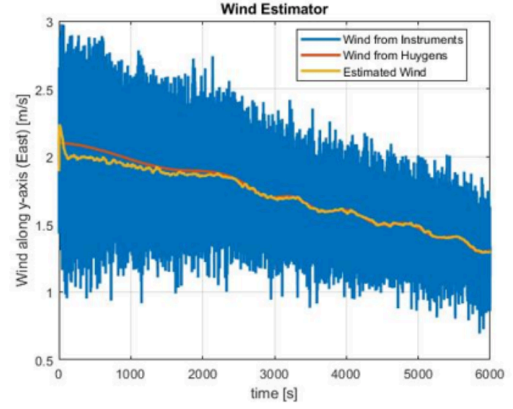

Figure 9. Zonal wind estimation on Titan.

Figure 10. Meridian wind estimation on Titan.

During the flight the density would be estimated from the sensors, so we should add some noisy measurements even in that case. The density derives from an exponential formulation that depends on the height [14,16], as reported in equation (2). To introduce some randomness, we can again think to perturb the airspeed as in the Kalman filter or the height lecture used in equation (2). The first method is based on the perturbation of the reading from the radar altimeter. The system uncertainty can be approximated as 2-5% of the indicated height from measurement, we can obtain our value of uncertain density indication. In the GNC simulations we will use a "fading memory filter": it is a recursive method similar to the linear-polynomial Kalman filter, but with a simpler formulation (less computational burdensome) due to the constant gain value. For a first order filter, the gain β is equal to 0.8. The algorithm for the density estimator is as follows:

$$h_k = h_{k-1} + (1 - \beta) * (h_{measured} - h_{k-1})$$
$$h_{measured} = h_{dynamic\ model} + \sigma_{h_{error}}$$
$$= h_{dynamic\ model} * \begin{cases} 1.05\ if\ h > 5000 \\ 1.02\ if\ h < 5000 \end{cases}$$
$$\rho_k = \rho_{k-1} + (1 - \beta) * (\rho_{exponential\ model} - \rho_{k-1})$$

$$(12)$$

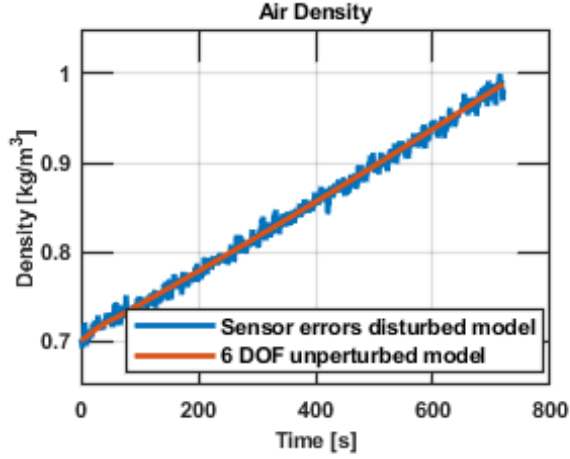Figure 11 shows the estimated density compared to the unfiltered measurement.

9

Figure 11. Air density estimation on Titan. The unperturbed model comes from eq. (2). [14, 15]

10. MOTION PLANNING

The parafoil trajectory must be planned towards the nearest point of interest (near the entry point) [14]: we would need a quick generation of a feasible trajectory. Usually for PADs the trajectory is planned with a 3 DOF model on plane: the variables of interest are $\{x, y, \psi\}$. From the wanted trajectory a series of waypoints is then computed on plane. In our deployment situation (40 km at 22 m/s) we need to consider a more complex 3 DOF model that consider the sphericity of the planet. The model will generate a trajectory with $\{V_a, \gamma_a. \chi_a\}$ (airspeed, flightpath angle and heading angle) and ϕ_a (bank angle) as a control. From this path we will compute our waypoints identified by a (x, y, z) ternary. The final point of the trajectory is $\{x_f, y_f, z_f\}_{NED} = \{0,0,0\}_{NED}$: with this expedient it will be easier to find a simple expression for optimize the trajectory for minimum control or as a Dubin path. During path planning usually only the wind vector is assumed to be $W = \{W_x, 0, 0\}$ where the wind component along x is the strongest one. In the true simulated trajectory, the lateral wind and the wind gust will be considered. However, the controlled 6 DOF system should be able to contrast those inputs even with a discrete control.

The mathematical expressions used to define the waypoints are presented next. The complete formulation can be found in [12,14]. The kinematics is defined through the planet radius r, the latitude λ, the longitude Λ and the ternary $\{x, y, z\}$.

In this case the body is modelized as a point mass with lift, drag, lateral force and buoyancy force (L, D, Y, B). The variable are the airspeed and the airspeed related flightpath angle and heading angle, that usually differ from the flightpath angle and heading angle

associated to the NED quantities. However, in this formulation the body axis and the wind axis coincide. Throughout all the formulation the wind is accommodated in the control equations (13) as in [12]. The guidance equations are as follows:

$$\dot{r} = V_a * \sin(\gamma_a) = \dot{h}$$

$$\dot{\Lambda} = \frac{V_a * \cos(\gamma_a) * \cos(\chi_a)}{r * \cos(\lambda)}$$

$$\dot{\lambda} = \frac{V_a * \cos(\gamma_a) * \sin(\chi_a)}{r}$$

$$\dot{x} = V_a * \sin(\gamma_a) + w_x$$

$$\dot{y} = V_a * \cos(\gamma_a) * \cos(\chi_a) + w_y$$

$$\dot{z} = V_a * \cos(\gamma_a) * \sin(\chi_a) + w_z$$

$$\tan(\phi_a) = \frac{\dot{\chi}_b * r * Va}{r * g - Va^2}$$

$$\dot{\chi}_b = \frac{2 * V_a * \cos(\gamma_a) * \sin(\chi_{desired} - \chi_a)}{L}$$

$$L = k * \sqrt{(y_{target} - y)^2 + (x_{target} - x)^2}$$

(13)

L is used to scale the intensity of the heading angle considering the distance between target and parafoil. This quantity can be modified with the k parameter: with different k we will obtain different trajectory that keeps into account the wind and that are all potentially feasible. Varying that quantity and the wind environment and the bank angle control, we can shape our path and find different solution to landing site. To automate the process an optimal control with a minimization process is needed. From simulations seems that k should be equal to one in the energy management or terminal guidance phases where the distance between parafoil and target is small but can assume different values to shape the homing phase accordingly to a mission requirement or a scientific task. In the following simulations k is assumed equal to the unity, if not explicitly reported in the plots' description.

If we plan to arrive to a point at 30 km of distance from the release point a possible path can be seen in the

following figures. The parafoil is upwind in the homing phase, when the wind intensity decreases below 3 m/s at 10 km the system can perform more intense maneuvers and start to aim more effectively at the landing site and land downwind. Throughout all the trajectory the bank angle is limited in its intensity: we want a feasible trajectory for the system. For small PADs a continuous bank angle over 1 m/s can make the vehicle unstable and the 6 DOF model can experience some problems in following the planned path. To minimize the bank angle and land on point in every different scenario we would need to optimize our trajectory for minimum control. The trajectory presented in the previous figures is one possible trajectory with a strong bank angle limitation [27]. The turn maneuver can cause quicker altitude loss and a steep spiral for descent. It can be hard to follow with a discrete control, at least with a simple proportional control in time domain. With a more refined control theory we should be able to perform any kind trajectory. If we change the entry point keeping ($\phi_{a_{max}} = 0.7 \; rad/s$), we can plot different trajectories that will try to land at the target $\{x_f, y_f, z_f\} = \{0,0,0\}$ km. The entries point will lie on a circle of radius 5 km around the nominal entry point, $\{x_0, y_0, z_0\} = \{-30,30,40\}$ km. However, without an optimizing tool and with the bank angle limitation the landing spots will can be delimited in an ellipse of major axis of 4 km along x (northing) and a minor axis of 2 km along y (easting). The error in position at the entry point at 40 km will perturb the touchdown point, keeping all the other parameters equal. Future work will expand this analysis into a more detailed Monte Carlo analysis. Figure 12 shows the result of the three-DOF guidance trajectory with waypoints. Figure 13 shows the latitude and longitude of the planned trajectory. Figure 14 shows the three-DOF guidance dispersion varying only the entry point with a dispersion of 5 km around the nominal entry point. Figure 15 shows that the dispersion at touch-down stays between 15km East and 40km North.
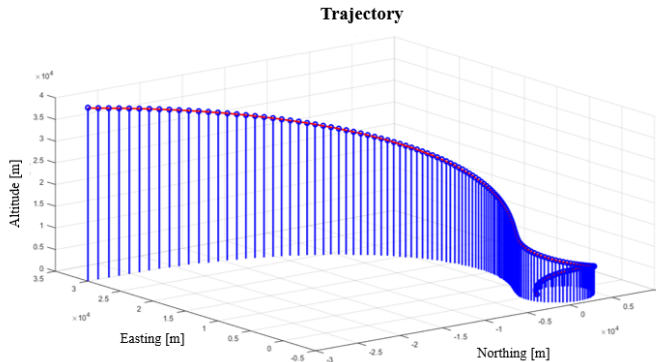
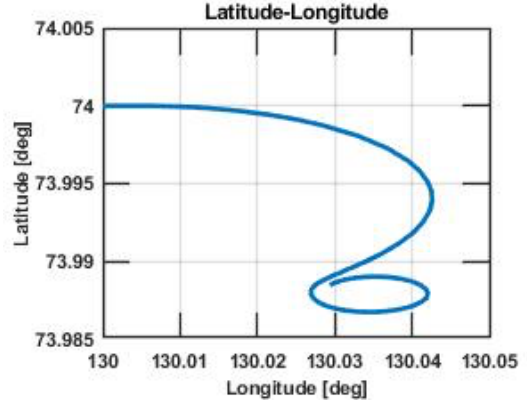Figure 12. Three-DOF guidance trajectory with waypoints.

Figure 13. Latitude and longitude of the planned trajectory.
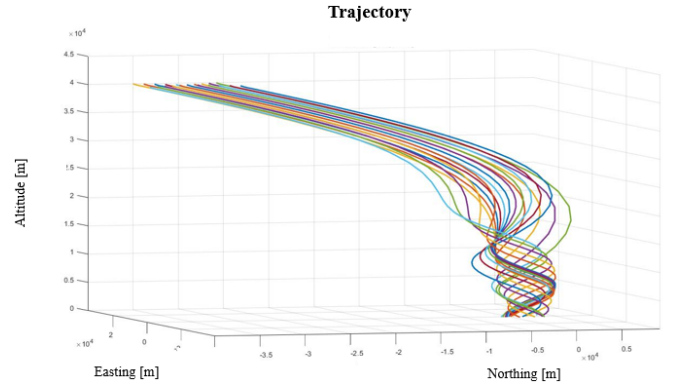

Figure 14. 3 DOF guidance dispersion varying only the entry point with a dispersion of 5 km around the nominal entry point.
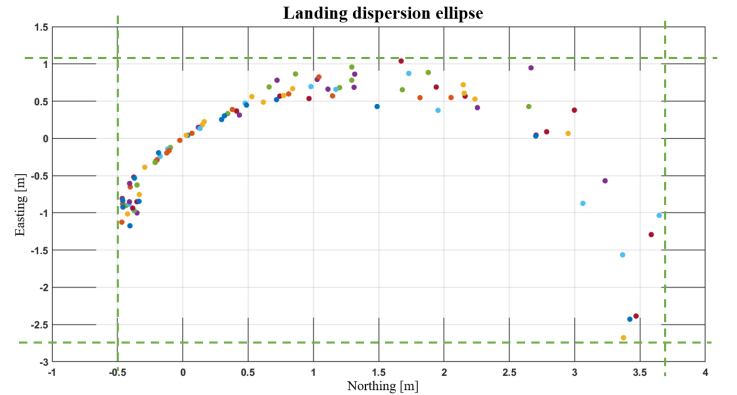

Figure 15. Dispersion at touch down.

11. CONTROL

The control used in the simulations is a simple fixed gain proportional control in time domain [14]. In this

preliminary phase we are not focused on the efficiency of the control but how the PADs will behave under some environmental effects, not precise sensor lectures and time-limited actuation. The control law is given by:

$$\delta_a = K_{p_2}(t)(\chi_{waypoint} - \chi_{parafoil})$$

$$(14)$$

The control will try to follow the on-plane trajectory (North-East). However, some waypoints cannot be reached because the 6 DOF PADs, with a more complex dynamics and various outside environmental effects, seems to lose altitude quicker than when it is modelled as a point mass object. If we follow the on-plane trajectory exactly we can land before our target. To obviate this problem the control algorithm aims always at the nearest waypoint with a lower height than the parafoil actual altitude. Figure 16 shows the projections of the trajectory in the horizontal and vertical planes and Figure 17 shows the comparison between the controlled and planned trajectories with the waypoints.
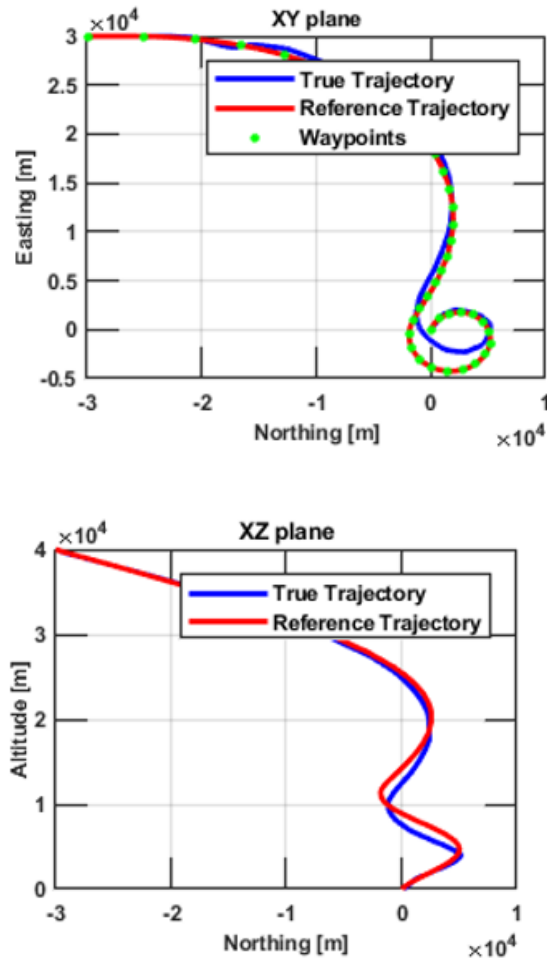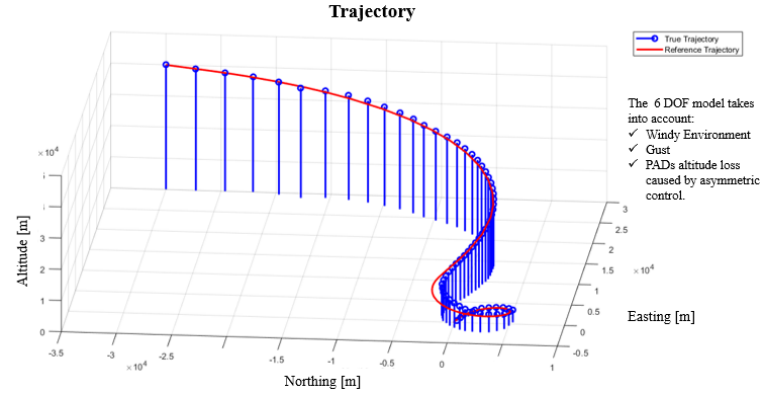

Figure 17: Controlled trajectory with waypoints.

12. DSENDS IMPLEMENTATION

JPL has developed the Dynamics Simulator for Entry, Descent and Landing (DSENDS) [30] as a high-fidelity spacecraft simulator for Entry, Descent, and Landing (EDL) on planetary and small astronomical bodies. The DSENDS software is an extension of a core set of software tools (Darts/Dshell) that is capable of modeling the dynamics of complex rigid and flexible multi-body systems. The core toolset is in use for multiple interplanetary and science-craft missions (Cassini, Galileo, SIM, and Starlight). DSENDS has been heavily used by Mars Lander missions to test precision landing and hazard avoidance functions for those missions. High-fidelity, physics-based engineering simulations of a spacecraft interacting with its environment are crucial in the analysis, development, test, validation, and operation of space flight missions. DSENDS is capable of simulating all critical phases of a space flight mission, which includes spacecraft ascent, orbit, deep space flight, rendezvous, proximity operations, atmospheric EDL, and planetary surface mobility. The DSENDS simulator incorporates physics-based models for articulated multi-body systems with flexible modes, aerodynamics, environments such as gravity, the atmosphere and planetary topography, spacecraft devices, and on-board flight guidance, navigation and control. The simulator allows the user to set up multi-spacecraft and mission configurations using elements from a modular library of components. Simulation parameters may be selected from a dispersed set to determine variations in trajectories for either Monte Carlo or parametric analysis. JPL routinely conducts Monte Carlo simulations of end-to-end EDL performance to assess delivery errors, including TRN for Mars precision landing. We have extended DSENDS libraries of vehicle dynamics models to handle the multi-stage

Figure 16: Six-DOF parafoil trajectory in the GN&C.

parachute concept proposed here and the specific state estimation, tracking, and control capability in conditions relevant to Titan's environment. TRN estimation is based on a SLAM-MSCKF algorithm and is a key component in this study for determining lander delivery error. For simulation purposes, the TRN estimation is carried out independently from the DSENDS simulation on a Robot Operating System (ROS) node. DSENDS publishes camera and IMU model data while it simultaneously listens for state estimates over the ROS node. Monte Carlo simulations will be used to study the dispersion of various design parameters for estimation and optimization of lander deliver error. This tool will be available for future Titan precision landing studies with different design points. Figure 18 shows a snapshot of the of the six-DOF DSENDS simulation.
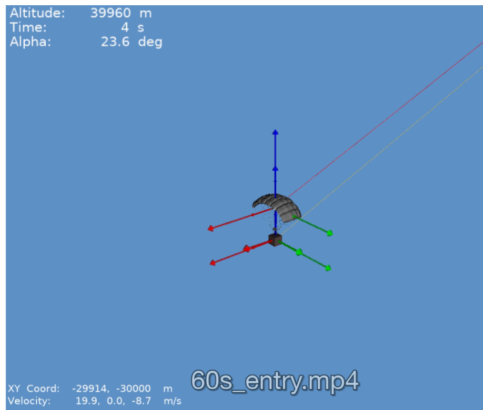

Figure 18. Snapshot from DSENDS simulation.

13. SUMMARY

We have developed and tested several dynamic models of a parafoil system descending in Titan's atmosphere. We are currently expanding these dynamic models to enable higher fidelity descent simulations to assess the impact on the landing precision using TRN estimation. In these models, we have included wind models used for Titan simulation, and extrapolated wind gust models previously used for simulation in the Martian environment. We have also developed guidance and control techniques to autonomously land the system. Finally, and in order to improve the controller performance by reducing the uncertainty to environmental factors, we have also developed ways to estimate the Titan environmental parameters, i.e. the atmospheric density, and the wind magnitude, during the descent. A more complete and realistic simulation is being developed, which uses JPL's DSENDS Entry, Descent, and Landing Software framework.

REFERENCES

[1] J.-P. Lebreton et al., "An overview of the descent and landing of the Huygens probe on Titan", *Space Science Reviews,* 104, 59-100, 2002

[2] *JPL Team X Titan Lake Probe Study Final Report,* Mission Concept Study for the Planetary Science Decadal Survey, 2010

[3] S. Leutenegger, S. Lynen, M. Bosse, R. Siegwart, P. Furgale: Keyframe-based visual-inertial odometry using nonlinear optimization. International Journal of Robotics Research, 34(3), 314-334. 2015.

[4] B. Kazeminejad et al., "Huygen's entry and descent through Titan's atmosphere -- methodology and results of the trajectory reconstruction," Planetary and Space Science, 55, 1845-1876, 2007

[5] Y. Dzierma et al., "Huygens probe descent dynamics inferred from Channel B signal level measurements," Planetary and Space Science, 55, 1886-1897, 2007

[6] *Data Archive Users' Guide for the Descent Imager and Spectral Radiometer (DISR) on the Huygens Probe*, 2013

[7] M. G. Tomasko et al., "The descent imager/spectral radiometer (DISR) experiment on the Huygens entry probe of Titan", *Space Science Reviews,* 104, 469-551, 2002

[8] N. J. Hughes, "Huygens proximity sensor design report," Technical report by Ylinen Electronics Co., 1994

[9] R. Trautner et al., "FMCW radars for entry probes and landers: lessons learned from the Huygens radar altimeter," *Proc. 3rd International Workshop on Planetary Probes*, 2005

[10] J. W. Barnes, R. H. Brown, J. M. Soderblom, L. A. Soderblom, R. Jaumann, B. Jackson, S. Le Mouelic, C. Sotin, B. J. Buratti, K. M. Pitman, K. H. Baines, R. N. Clark, P. D. Nicholson, E. P. Turtle, J. Perry, J., 2009. Shoreline features of Titan's Ontario Lacus from Cassini/VIMS observations. Icarus 201, 217-225.

[11] M. San Martin, G. Mendeck, P. Brugarolas, G. Singh, F. Serricchio, S. W. Lee, E. C. Wong, J. C. Essmiller, 2015. In-flight experience of the Mars Science Laboratory guidance, navigation, and

control system for entry, descent, and landing. CEAS Space Journal, 7(2), 119-142

[12] M. B. Quadrelli: "A Novel Approach to Planetary Precision Landing using Parafoils." Advances in the Astronautical Sciences 120 (2005): 229-244.

[13] M. B. Quadrelli, and A. B. Acikmese: "Planetary Aeromaneuvering for precision landing" Advances in the Astronautical Sciences 120 (2005)

[14] O. A. Yakimenko: " Precision Aerial Delivery Systems: Modeling, Dynamics, and Control" AIAA, Volume 248 Progress in Astronautics and Aeronautics, 2015.

[15] R. D. Lorenz.:" Attitude and angular rates of planetary probes during atmospheric descent: Implications for imaging." Planetary and Space Science 58.5 (2010): 838-846.

[16] R. Yelle, D. Strobell, E. Lellouch, D. Gaultier, "Engineering Models for Titan's Atmosphere".

[17] R. D. Lorentz and e. al, "Formulation of a wind specification for Titan late polar summer exploration.," in Planeary and Space Science, Elvesier, 2012, pp. 73-83.

[18] T. Jann: "Aerodynamic Coefficients for a Parafoil Wing with Arc Anhedral: Theoretical and Experimental Results." AIAA Paper 2106 (2003): 19-22.

[19] P. Lissaman, G. Brown, "Apparent mass effects on parafoil dynamics", Aerospace Design Conference. 1993.

[20] T. Melin, "User's Guide Tornado 1.0", Royal Institute of Technology (KTH), 2001.

[21] W. Gockel: "Computer Based Modeling and Analysis of a Parafoil-Load Vehicle, case study 1." Seminar at 14th AIAA ADS Conference, San Francisco. 1997.

[22] C. Toglia, M. Vendittelli, Marilena: "Modeling and motion analysis of autonomous paragliders", Technical Report. Department of Computer and System Sciences Antonio Ruberti, Roma, 2010.

[23] N. J. Slegers and C. M. Gorman, "Comparison and Analysis of Multi-body Parafoil Models with Varying Degrees of Freedom," in American Institute of Aeronautics and Astronautics, 2011.

[24] N. Ananthkrishnan and P. Om, "Modeling and Simulation of 9 DOF Parafoil-Payload System Flight Dynamics," in AIAA Atmospheric Flight Mechanics Conference and Exhibit, Keystone, Colorado, August 2006.

[25] L. Ermolli: "Flight Maneuvering for Planetary Landing on Titan", M.S. Thesis, Politecnico of Milano, 2018.

[26] J. Rimani: "High-Lift Systems for Planetary Descent and Landing", M.S. Thesis, Politecnico of Torino, 2018.

[27] M. Nitin et al, "Guidance of Parafoil using Line of Sight and Optimal Control", Kampur, 2014.

[28] J. M. Stein, C. M. Madsen, A. L. Strahan: 2005. An overview of the guided parafoil system derived from X-38 experience. 18th AIAA Aerodynamic Decelerator Systems Technology Conference and Seminar

[29] B. J. Rademacher: In-flight trajectory planning and guidance for autonomous parafoils. PhD thesis, Iowa State University, 2009.

[30] J. Balaram, R. Austin, P. Banerjee, T. Bentley, D. Henriquez, B. Martin, E. McMahon, G. Sohl: "DSENDS - A High-Fidelity Dynamics and Spacecraft Simulator for Entry, Descent and Surface Landing," IEEE 2002 Aerospace Conf., Big Sky, Montana, March 9-16, 2002.

BIOGRAPHY

Marco Quadrelli is an internationally renowned expert in modeling for dynamics and control of complex space systems. He has a Master Degree in Aeronautics and Astronautics from MIT and a PhD in Aerospace Engineering from Georgia Tech. He was a visiting scientist at the Harvard-Smithsonian Center for Astrophysics, and a lecturer at the Caltech Graduate Aeronautical Laboratories. After joining NASA JPL in 1997 he has contributed to a number of flight projects including the Cassini---Huygens Probe, Deep Space One, the Mars Aerobot Test Program, the Mars Exploration Rovers, the Space Interferometry Mission, the Autonomous Rendezvous Experiment, and the Mars Science Laboratory, among others. He has been the Attitude Control lead of the Jupiter Icy Moons Orbiter Project, and the Integrated Modeling Task Manager for the Laser Interferometer Space Antenna. He has led or participated in several independent research and development projects in the areas of computational micromechanics, dynamics and control of tethered space systems, formation flying, inflatable apertures, hypersonic entry, precision landing, flexible multibody dynamics, guidance, navigation and control of spacecraft swarms, terramechanics, and precision pointing for optical systems. He is an Associate Fellow of the American Institute of Aeronautics and Astronautics, a NASA Institute of Advanced Concepts Fellow, and a Caltech/Keck Institute for Space Studies Fellow.

Jasmine Rimani is a space engineering graduate student at the Politecnico di Torino. She's interested in space related flight mechanics and guidance, navigation and control. She has been an intern in the aerothermodynamic division of ESA-ESTEC. Where she worked on reusable launchers preliminary design. She wrote her master thesis at JPL-NASA on the dynamics and GN&C of autonomous high-lift systems for planetary explorations. She is working on the development of a GN&C software for a Lunar Space Tug with electric propulsion in collaboration with the Politecnico di Torino.

Luca Ermolli is a Space engineering graduate student at Politecnico di Milano. He has been an intern at NASA-JPL robotic section, where he worked on the dynamics and control of autonomous parafoils for space exploration. He is interested in modeling and simulation of aerial and space vehicles, with focusing on flight mechanics and attitude control. Currently he is working in Italy for the Leonardo Helicopters Flight Mechanics department.

Aaron Schutte is a Robotics Systems Engineer in the Modeling and Simulation Group at NASA JPL where he supports the development of advanced high-fidelity multi-mission simulation tools in the DARTS Lab. Prior to joining JPL he worked as a researcher in the Vehicle Systems Division at The Aerospace Corporation developing computational tools and algorithms for analysis of spacecraft GN&C systems and GPS. His primary contributions are in the development of high fidelity rigid and flexible multibody simulations, spacecraft control design and estimation techniques, and development of automatic derivative methods. He is a Senior Member of the AIAA and has served as a regular member of the AIAA GN&C Technical Committee.